Recognizing real materials from their glossy appearance

Guillaume Ged, Gaël Obein, Zaccaria Silvestri, Jean Le Rohellec, F. Vienot

Recognizing real materials from their glossy appearance

Guillaume Ged — Propriétés Optiques des Matériaux, Laboratoire Commun de Métrologie LNE-Cnam, La Plaine Saint-Denis, France, & Centre de Recherche sur la Conservation des Collections CNRS USR 3224, Muséum National d'Histoire Naturelle, Paris, France

Gaël Obein — Propriétés Optiques des Matériaux, Laboratoire Commun de Métrologie LNE-Cnam, La Plaine Saint-Denis, France

Zaccaria Silvestri — Equipe Masse et Grandeurs Associées, Laboratoire Commun de Métrologie LNE-Cnam, La Plaine Saint-Denis, France

Jean Le Rohellec — Centre de Recherche sur la Conservation des Collections CNRS USR 3224, Paris, France

Françoise Viénot — Centre de Recherche sur la Conservation des Collections CNRS USR 3224, Muséum National d'Histoire Naturelle, Paris, France

In everyday life, the visual system is remarkably good at recognizing materials across a wide range of viewing conditions. This paper addresses the problem of identifying real samples of materials from appearance. Here, we consider gloss as an appearance attribute that could reveal certain information about object properties. We prepared twelve samples of glass and PMMA and eroded these using different agents. The gloss and haze of the samples were measured at 60 degrees via a gloss meter. For all samples, the surface roughness properties were measured. Microfacet distributions were derived from measured BRDFs using an inverted microfacet model. We conducted a visual ranking experiment using the pair comparison method. The psychophysical gloss ratings correlate well with the 60 degrees gloss index. Principal component analysis of the psychophysical results revealed a somewhat more complicated picture in which three components seem to play a role. We conclude that observers can apprehend the physical nature of the surface of real objects from features that are included in the BRDF and available in the gloss appearance.

Keywords: gloss, material roughness, multidimensional visual scaling, BRDF

Citation: Ged, G., Obein, G., Silvestri, Z., Le Rohellec, J., & Viénot, F. (2010). Recognizing real materials from their glossy appearance. *Journal of Vision, 10*(9):18, 1–17, http://www.journalofvision.org/content/10/9/18, doi:10.1167/10.9.18.

Introduction

In everyday life, the visual system is remarkably good at recognizing materials across a wide range of viewing conditions. This paper addresses the problem of identifying real samples of materials from appearance. Here, we consider gloss as an appearance attribute that could reveal pieces of information about object properties.

We conjecture that gloss discloses pieces of information that the visual system collects, classifies, and identifies.

General

Gloss is an appearance attribute that originates from the directional distribution of luminances reflected from the surface.

From a perceptive point of view, gloss can be considered as a "second-order" visual attribute. It results from an interpretation by the brain of first-order signals, such as simple luminance variations. In order to evaluate the gloss of a surface, an observer needs separate first-order signals. This implies that he must look at the surface of an object from two or more different angles to receive enough information to attribute a value to the gloss of that surface.

Recently, gloss has received attention as an appearance attribute. Using a pair comparison technique with ten black coated samples, Obein, Knoblauch, and Viénot (2004) showed that the visual gloss scale was not linearly related to the corresponding gloss index obtained from a gloss meter. Furthermore, the comparison of data obtained using two different observing angles (60° and 20°) indicates that, although the flux that is collected by the

doi: 10.1167/10.9.18 Received March 15, 2010; published December 21, 2010 ISSN 1534-7362

eye varies according to the angle of view, an observer is able to recover a visual gloss index that is inherent to the surface. Obein et al. named this property gloss constancy. The profile of the visual gloss scale agrees with the one found by Ji, Pointer, Luo, and Dakin (2006). Another psychophysical experiment was conducted to investigate the differential gloss threshold variation or so-called just noticeable difference (Ng et al., 2003). Within the investigated gloss range—gloss index from 10 to 60—gloss perception follows the Weber's Law, which led the authors to emphasize the similarities between gloss and light intensity perception.

The dimension of gloss

Nevertheless, gloss perception is neither simple nor unique. Hunter and Harold (1987) have defined a number of gloss descriptors: specular gloss, sheen, contrast gloss or luster, absence of bloom, and distinctness of image (DOI; Smith, 1997). Besides specular gloss descriptor, Pointer (Commission Internationale de l'Eclairage (CIE), 2006) retained the distinctness of image when an image reflected in the surface appears sharp, and the haze (that is the inverse of absence of bloom) or the contrast gloss when an image reflected in the surface appears of low contrast.

These different classes raise the question of the dimensionality of gloss, which is still under debate. In an experimental study using real painted achromatic panels, with a wide range of gloss, Billmeyer and O'Donnell (1987) concluded that their observers could not reliably distinguish more than one dimension, although the output of multidimensional scaling could give for the second dimension a "folded" gloss scale that had no obvious interpretation. Pellacini, Ferwerda, and Greenberg (2001) simulated white gray and black painted spheres and checkerboards by adjusting the three parameters of the isotropic Ward reflection model to approximate measured BRDFs. They asked subjects to estimate the apparent difference in gloss between pairs of objects. Multidimensional scaling revealed that under these conditions apparent gloss has two dimensions that they could relate to the apparent contrast of the reflected image (contrast gloss) and the distinctness of the reflected image (DOI). In a large study, 75 participants performed paired comparisons of rendered images with constant geometry and illumination and with varying BRDFs (Wills, Agawal, Kriegman, & Belongie, 2009). The authors used a multidimensional scaling algorithm for analyzing pairwise comparisons. They could extract nine gloss dimensions.

The BRDF

From an optical point of view, the physical information relevant to gloss is provided by the bidirectional reflectance distribution function (BRDF). This function completely describes the distribution of the light reflected by the surface of an object. By definition, it is expressed as the ratio of the reflected radiance $L_{\mathbf{R}}$ exiting the surface to the incident irradiance $E_{\mathbf{I}}$, for given incident direction $\mathbf{I}$ and exiting direction $\mathbf{R}$ (cf., Equation 1 and Figure 1):

$$\mathrm{BRDF}(\psi, \varphi_{\mathbf{I}}, \theta, \varphi, \lambda) = \frac{\mathrm{d}L_{\mathbf{R}}(\psi, \varphi_{\mathbf{I}}, \theta, \varphi, \lambda)}{\mathrm{d}E_{\mathbf{I}}(\psi, \varphi_{\mathbf{I}}, \lambda)}. \quad (1)$$

Acquiring BRDFs of real materials is a time-consuming process and provides a large quantity of data that are difficult to manipulate. After the measurement, the classic way to proceed is to use a model in order to represent a large number of measurement data by a small number of parameters. In recent years, there has been a lot of effort in proposing different models for the BRDF (Blinn, 1977; Gouraud, 1971; Matusik, Pfister, Brandy, & McMillan, 2003; Phong, 1975; Torrance & Sparrow, 1967; Ward, 1992).

The use of these models of BRDF in computer graphics makes it possible to render the appearance of many natural surfaces such as velvet or peachy skin, but we do not know which parameters should be extracted from the BRDF to be perceptually meaningful with respect to real materials (Koenderink & Pont, 2003). The link between the visual perception of gloss and the BRDF is still missing.

Recovery of material

Viénot and Obein (2004) compared the BRDF of two matte planar materials: a piece of tire rubber with a piece of black coated cardboard. While the areas enclosed by the plot of both specular peaks are about the same size, the curves cross several times. The crossovers precisely illustrate the visual percept: when the two samples are viewed at grazing angles, or at specular angle, the piece of rubber appears brighter than the coated paper, while when

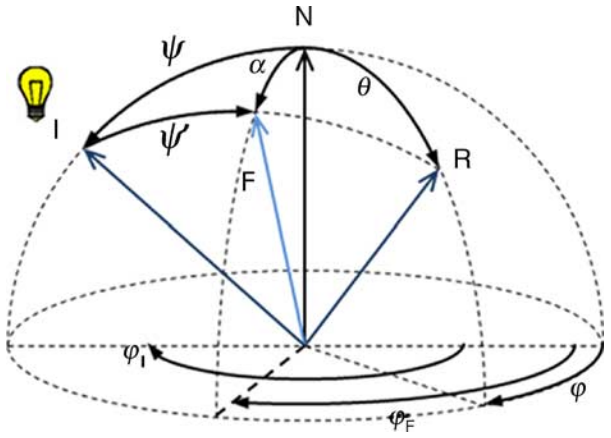

Figure 1. Geometry of the BRDF.

the two samples are viewed around the peak, it appears darker (see Figure 2).

This could explain why an observer must look at an object from two or more different angles to recover enough information to be able to identify the surface. He might be looking for specific indices (Delaney, de la Rie, Elias, Sung, & Morales, 2008). We conjecture that an active strategy could allow the subject to recognize the visual cues that provide the necessary information to identify the material an object is made of.

Among the cues that could explain our ability to recover information about the material an object is made of are gradients in color and luminance, which actually relate to the shape of the BRDF. Several investigators have verified that observers are able to distinguish between luminance gradient profiles (Bloj, Kersten, & Hurlbert, 1999; Garcia-Suarez, Ruppertsberg, & Bloj, 2008; Ruppertsberg, Bloj, & Hurlbert, 2008; Viénot, Boust, Brémond, & Dumont, 2002). Using digital images, Motoyoshi, Nishida, Sharan, and Adelson (2007) suggest that the recovery of glossiness could be attributed to the skewness of the pixel distribution. Motoyoshi et al. (Motoyoshi, Nishida, & Adelson, 2005; Motoyoshi et al., 2007) showed that given an image of a textured surface, skewing the pixel luminance histogram alters its appearance either to matte when skewed negatively (a predominance of decrements) or to glossy when skewed positively (a predominance of increments).

Another area of investigation is the coherence between the localization of the light source, the diffuse, and the specular components. For some authors, when the diffuse and specular components of luminance are independently manipulated, observers are able to disentangle highlights, surface lightness, and surface color of 3D objects (Todd, Norman, & Mingolla, 2004; Xiao & Brainard, 2008). Fleming, Dror, and Adelson (2003) showed that subjects could estimate surface reflectance reliably and accurately in the absence of context, as long as the illumination was realistic. For other authors, even in ecologically valid images of complex objects, the perception of material, the perception of shape, and illumination are basically confused (te Pas & Pont, 2005; Vangorp, Laurijssen, & Dutré, 2007).

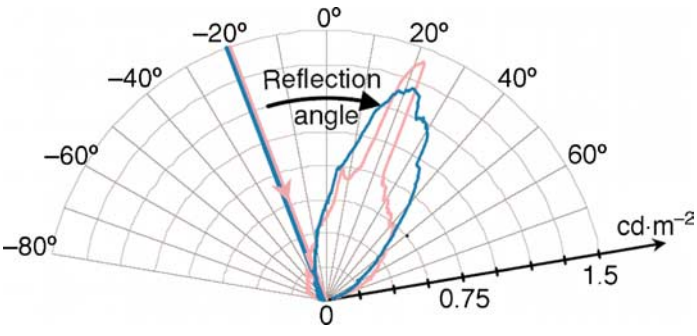

Figure 2. Specular peaks of two materials: the pink curve stands for the rubber sample, the blue curve for the coated paper (Viénot & Obein, 2004).

How the subjects have acquired knowledge of the cues that exist as to what is light and what is material is still unknown (Landy, 2007).

Objectives

The visual system is remarkably good at recognizing materials across a wide range of viewing conditions. As long as the BRDF is correctly rendered, and the layout is similar to what could be found in a real and natural context, the visual system gives the right interpretation. Moreover, no matter what is modified in the BRDF—the direction of illumination, the direction of observation, the roughness—the visual system finds a realistic appearance solution in which all physical parameters are in harmony. Whereas the previous studies with computer graphics techniques focused on "what should be put in the BRDF in order to display objects that look realistic," here we propose to investigate "what is picked up in the real BRDFs by the visual system to recognize and identify real materials." Assuming that the richest part of the BRDF, in terms of information about the surface roughness and material properties, is the specular peak and its neighborhood, we worked on gloss appearance. We designed a psychophysical experiment to identify which quantities are relevant to the visual system to describe the gloss perceptual space. Then, we confronted these perceptual quantities and the BRDF measurements in order to see what the visual system takes in the BRDF to identify materials.

Methods

To answer these questions, we set up a psychophysical experiment where the observers were presented with different materials that produce different shapes of the specular peak. Two black materials were depolished using two different processes to create a range of samples with different specular peaks. We measured the roughness and BRDFs of the samples and modeled the BRDFs by fitting a microfacet model. Observers were then asked to rate the glossiness of the samples. Finally, we performed multidimensional analysis of the visual results to extract perceptual cues and we looked for correlations between psychophysical and optical data.

Equipment

Samples

We have intentionally restricted our study to the quantification of the visual perception of gloss for black samples. The advantage of using black samples is that it is

only the surface reflection that is responsible for the appearance of the surface. The absence of volume or subsurface diffusion from black samples makes the observation of highlights due to the surface reflection prevail. For this reason, black samples allow us to study accurately the sensitivity of the visual system to luminous variations associated with surface reflection.

We wanted to investigate the effects on gloss perception of modifying the shape and height of the specular peak. This aim has led us to use bulk material samples with different optical indices and different roughness.

In a former experiment using black coated samples (Obein et al., 2004), we showed that the visual gloss judgments were practically unaffected by the geometry of illumination. Thus, in order to exploit the poor differential sensitivity and the variability of the observers' responses, we limited the range for this study between 50 and 80 gloss units (gu) measured with a gloss meter in the 60° configuration.

In order to carry out comparisons, three scales of four samples each were created. Two scales were created with black polymethylmethacrylate (PMMA)—commonly known under the name Plexiglas—with pallets of 75 × 50 × 4.5 mm. The pallets' transmittance was tested with a 633-nm laser beam and it was shown that these were opaque (Coutin, 2010). Native PMMA samples are highly reflective. Two separate methods were used to depolish these samples, a physical and a chemical one. The physics-based process consisted in plunging the mirror-like sample inside a bath of alumina shards in motion. The longer the sample remained exposed to this bath, the more matte it became. Four PMMA sanded samples were created. These samples are labeled P1 to P4 from the rougher to the glossier. The second scale was based upon a chemical attack of the surface. Acetonitrile is a solvent for many plastics, including PMMA. Four levels of gloss were obtained by controlling the exposure time of the samples to this product. These samples are labeled C1 to C4 from the rougher to the glossier. The third scale was built from Neutral Grey 9 Schott glass (NG9), which can be assumed to be opaque under indoor illumination (Transmittance $T \approx 10^{-5}$). Four raw black glass samples of equal dimensions to the PMMA pallets were eroded using random polishing to obtain a mirror-like appearance and then submitted to repeated alumina-eroding treatments. These samples are labeled Gl1 to Gl4 from the rougher to the glossier.

Gloss and haze measurements

The measurement of specular gloss for nonmetallic surfaces is standardized for three particular incident angles (20°, 60°, and 85°). The specular gloss, expressed in gloss unit (gu), is given by the ratio of the flux reflected, in a given aperture centered on the specular direction, at the surface of the sample in relation to the flux reflected at the surface of a standard (in the same conditions). The standard is a piece of polished black glass having a refractive index n = 1.567 (ISO 2813, 1978). Specular gloss measurements at 60° were made using a ZLR 1050 Zethner gloss meter upon ten different points of the plates.

According to the ASTM standard related to high gloss surface (ASTM E430-97, 1997), haze *is, for a specified specular angle, the ratio of flux reflected at a specified angle (or angles) from the specular direction to the flux similarly reflected at the specular angle by a specified gloss standard.*

Haze values were obtained with the Zethner equipment, using a dedicated measuring head. These are expressed in relative value with respect to a ceramic standard (reflection haze value = 380). The measurements are shown in Figure 3.

The eroding processes of PMMA samples were controlled by monitoring the exposure time. The samples were labeled according to their gloss indices, to obtain uniform scales.

Glass needed longer exposure to the alumina bath to induce gloss variation. While data issued from the gloss meter were constant, the longer the glass was exposed, the more the visual aspect of the samples changed. Consequently, the glass scale was developed by controlling the time of erosion from visual inspection.

Surface microscopy

Images from the depolished surfaces (Figure 4) were obtained due to a video microscope, using a coaxial

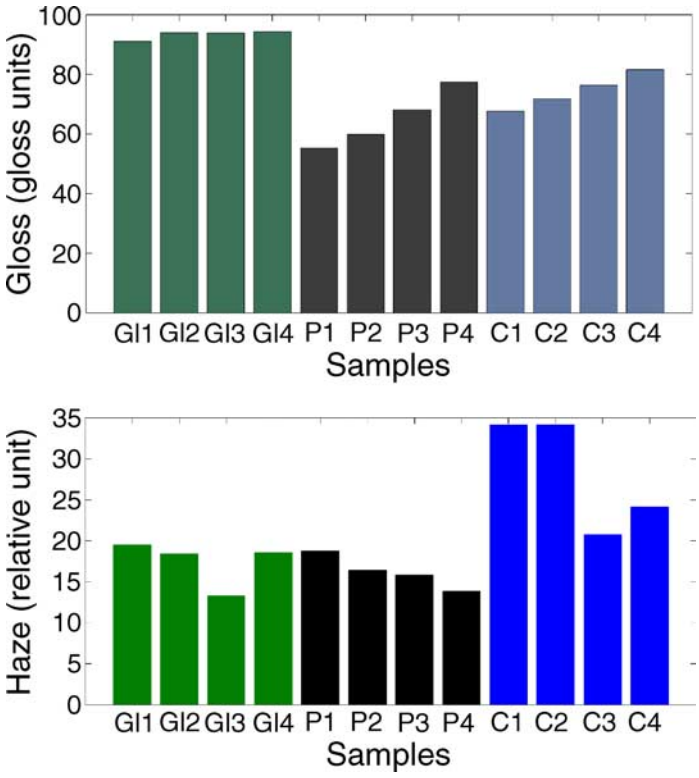

Figure 3. Gloss index and haze index measurements.

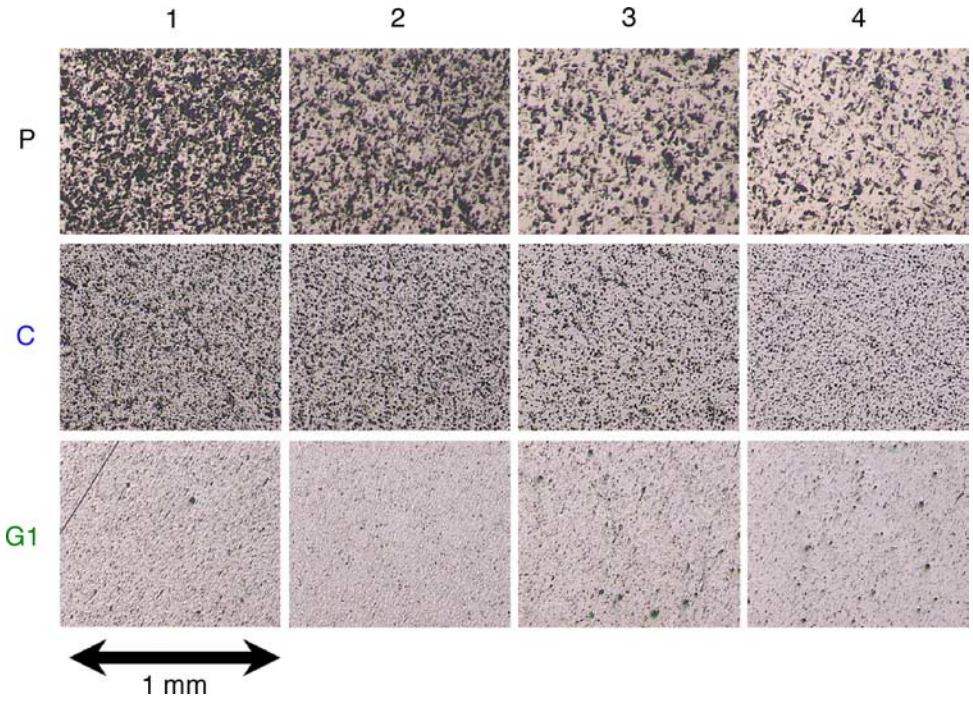

Figure 4. Microphotographs of the three sets of samples. Upper row shows physically eroded PMMA samples; middle row shows chemically eroded PMMA samples; lower row shows physically eroded glass samples. Gloss index increases from left to right.

illumination with 4.5× magnification. The apparatus consists of a compact optical system Optem Zoom 65, allowing magnifications between 0.7× and 4.5×, with possibility of coaxial illumination of exposed surfaces. Image rendering was possible through a color camera Sony SSC-DC58AP and a CRT monitor.

Figure 4 shows that the microscopic aspect of each set of samples is different in nature. Particularly, the physical and the chemical PMMA present different types of asperities. The alumina eroding digs up shards of bulk material and the chemical attack produces smooth craters in it. These assumptions have been confirmed on a qualitative perspective by profilometry and interferometric microscopy over two PMMA samples (see Appendix A). A variation in magnitude with respect to the gloss index can be seen on pictures from the same set.

Surface roughness

An optical roughness meter (Zerrouki, 1998) was used to characterize the surface roughness of each sample. This technique consists in measuring the distribution of scattered intensity in the incident plane to determine the power spectral density (PSD) of surface roughness. From this PSD, the root mean square height is extracted.

A small surface element (about 1 mm^2) is illuminated under oblique incidence (about 46°) by p-polarized monochromatic light (wavelength, λ = 632.8 nm). Then, measurements of the angular distribution of the scattered light are made at several sites within the plane of incidence on the sample surface (see Figure 5). By using the angle-resolved scattering theory (Elson & Bennett, 1979; Kröger & Kretschmann, 1970), this distribution is related to the surface roughness (through the power spectral density—PSD).

Each sample was analyzed in 5 representative sites. The mean PSD curves for each sample of the three scales are presented in a log–log scale in Figure 6. Two additional samples were analyzed in order to complete the interpretation of the PSD curves: a native PMMA sample (P0) and a polished glass sample (Gl0) that had not been sanded. The results confirm observations made with the video microscope.

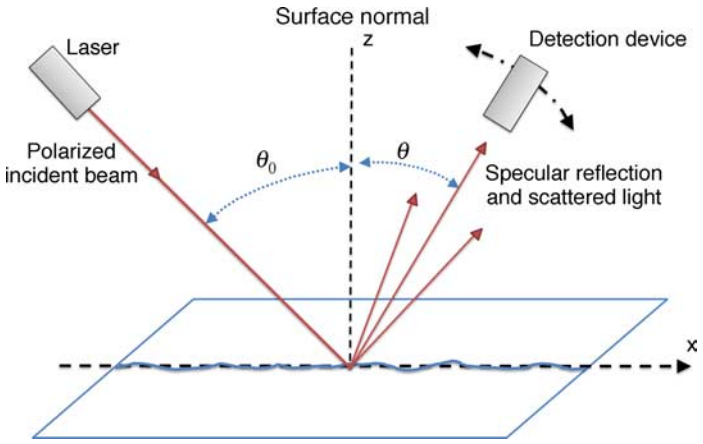

Figure 5. Illustration of the scattering geometry.

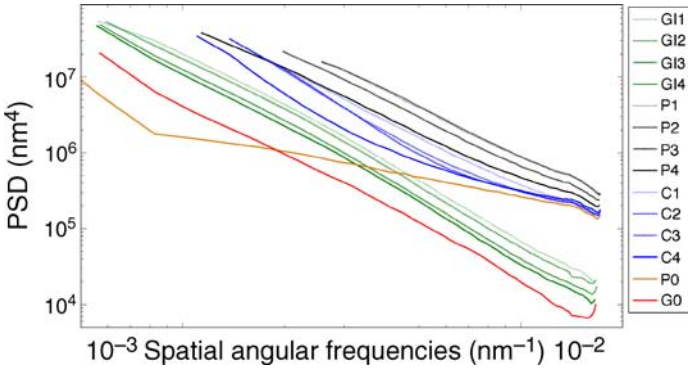

Figure 6. Power spectral density for each sample according to the spatial frequency (log–log scale). Black curves stand for P-PMMA scale (Pi), blue for C-PMMA scale (Ci), green for glass scale (Gli), and orange and red curves from raw samples of PMMA and glass.

The sanded PMMA (P-PMMA), the chemically attacked PMMA (C-PMMA), and the glass scales are clearly separated by the optical scattering measurements. The PSD curves are indeed characteristic of each scale of materials. With the lowest PSD amplitude, the glass scale is less rough than the PMMA scales. In fact, the rms height (in a band of angular spatial frequencies extrapolated from 0 to infinity) stretches from 14 to 18 nm, 32 to 40 nm, and 26 to 31 nm, respectively, for the glass scale, the chemical PMMA scale, and the physical PMMA scale.

PSD shows the signature of each process as well:

1. Regarding the polished glass and the P-PMMA scales, the number of alumina-eroding cycles increases the surface roughness. The result of this process can be seen as similar to white noise acting over all spatial angular frequencies and shifting the PSD curves up (black and green curves in Figure 6). We note that the PSD slopes of the P-PMMA and glass scales are quite similar, marking the signature of the eroding process.
2. Regarding the C-PMMA samples, the curvature of the PSD function is accentuated by the chemical erosion and no obvious shift of the PSD curve is observed for high spatial angular frequencies. This is because the treatment favors certain frequencies over others. Indeed, for spatial angular frequency above 10^{-2} nm^{-1}, the chemical process has no effect on the superficial surface (blue curves in Figure 6).

BRDF measurements

BRDF measurements were carried out on each sample. The instrument we used was the EZ-Contrast 160 developed by ELDIM. This apparatus allows the illumination of the sample with a collimated light beam and a user-defined incident angle and measures the luminance reflected inside a ±80° cone of observation, with a narrow solid angle of approximately $1.5E^{-4}$ sr depending on the direction of observation. This system is based on a combination of Fourier Optics and a cooled CCD sensor head (Moreau, Curt, & Leroux, 2000). For a given incident direction, the EZ-Contrast records the luminance in the directions (θ, ϕ), with $0° < \theta < 80°$ and $0° < \phi < 360°$ in one shot. θ and ϕ vary with a step of 0.4°. As our samples are assumed to be isotropic, we used only one azimuth of illumination. Unfortunately, the equipment does not provide the illumination. Thus, we do not measure the BRDF rigorously, but only the distribution of the luminance, for a given illumination (unknown but constant).

We performed measurements for ten directions of illuminations (ψ = 20°, 30°, 35°, 40°, 45°, 50°, 55°, 60°, 65°, 70°). We performed 4 repetitions on different areas of the sample. An example of this measurement can be seen in Figure 7.

The microfacet modeling of the BRDF

The previous measurements give more than 1 million values of luminance for each sample. In order to reduce this enormous amount of data to a few relevant parameters, we have to model the measurements.

We used an in-house model (Obein, Leroux, Knoblauch, & Viénot, 2003), based on the microfacet approach proposed by Cook and Torrance (1982). The model has already been successfully applied to a gloss scale of ten items (Obein & Viénot, 2007).

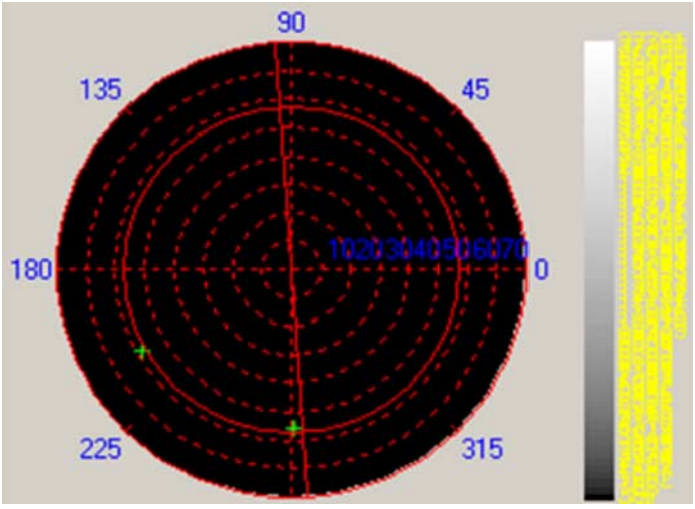

Figure 7. Measurement done using the EZ-Contrast. The studied sample is a physically eroded PMMA. The specular peak is located at the intersection of the circular continuous line and the diagonal line and is very narrow. This measurement shows the high level of gloss of our samples.

The model of Cook–Torrance is based on two hypotheses:

• Hypothesis 1:

It is assumed that the specular component and the diffuse component of the BRDF are independent. The BRDF is given by the summation of the two components:

$$\mathrm{BRDF}(\psi,\theta,\varphi)=\frac{1}{E_{\mathbf{I}}(\psi)}\left[L_{\mathrm{spec}}(\psi,\theta,\varphi)+L_{\mathrm{diff}}(\psi)\right]\ \left(\mathrm{sr}^{-1}\right), \tag{2}$$

where $E_{\mathbf{I}}(\psi)$ is the illumination at the zenithal angle ψ, $L_{\mathrm{spec}}(\psi,\ \theta,\ \varphi)$ is the luminance in the direction $\mathbf{R}(\theta,\ \varphi)$ coming from the specular component, and $L_{\mathrm{diff}}(\psi)$ is the luminance in the direction $\mathbf{R}(\theta,\ \varphi)$ coming from the diffuse component.

For our application, the diffuse component is negligible because the samples are black.

• Hypothesis 2:

The specular component is obtained by approximating the surface with a theoretical surface composed of microfacets, the statistical distribution of which depends upon the sample. The light reflection on the facets is assumed to be specular and to follow geometric optical laws (Torrance & Sparrow, 1967). Thus, the specular component is given by

$$L_{\mathrm{spec}}=\frac{E_0}{\Omega}\cdot\frac{\cos\alpha}{\cos\theta}\cdot F(n,\psi')\cdot G(\psi,\theta,\alpha,\psi')\cdot P(\alpha)\left(\mathrm{cd\ m}^{-2}\right), \tag{3}$$

where E_0 is the illumination along $\mathbf{N}$ (see Figure 1); Ω is the collection solid angle; $F(n,\ \psi')$ is the Fresnel factor depending on n (the refractive index of the material) and ψ' (the angle of incidence of the light on the microfacet); $G(\psi,\ \theta,\ \alpha,\ \psi')$ is a function that takes into account the masking/shadowing of the adjacent facets; $P(\alpha)$ is the microfacet angular distribution function.

The function $P(\alpha)$ describes the probability of finding a facet oriented with a given normal $\mathbf{F}$. As our surfaces are isotropic, the probability depends only on the zenith α. The choice of the function to be used has been discussed several times (Blinn, 1977; Cook & Torrance, 1982; Obein, Leroux, Knoblauch, & Viénot, 2001). All these propositions are mathematical functions that are independent of the material. In our model, we use a function that is derived from the BRDF measurements, by inverting the model. The method is described below.

From our measurements, we obtained the values of the luminance reflected by the sample in the half-space, for 10 different angles of illumination. As we said previously, our equipment does not provide information about E_0, the absolute value of the illumination. Furthermore, the value of the solid angle Ω by which 1 pixel of the CCD is seen by the surface is not well known. However, we know that E_0 and Ω are independent of the directions of illumination and reflection. We define C_{spec} by

$$C_{\mathrm{spec}}=E_0/\Omega\quad\left(\mathrm{lm\ m}^{-2}\ \mathrm{sr}^{-1}\right), \tag{4}$$

where C_{spec} is a constant of the equipment.

Equation 3 becomes

$$L_{\mathrm{spec}}=C_{\mathrm{spec}}\cdot\frac{\cos\alpha}{\cos\theta}\cdot F(n,\psi')\cdot G(\psi,\theta,\alpha,\psi')\cdot P(\alpha)\quad\left(\mathrm{cd\ m}^{-2}\right). \tag{5}$$

In this equation, only $P(\alpha)$, C_{spec}, and n are unknown.

We determine the unknown in 3 steps:

Step 1: Adjustment of the refractive index n from the measurements made in the plane of incidence.

As we know the value of the luminance in the plane of incidence, we can reverse Equation 5 and express the product $C_{\mathrm{spec}}\cdot P(\alpha)$ according to the measurements and an arbitrary refractive index, for each direction of illumination where the measurements were performed. As $P(\alpha)$ is a characteristic of the sample and C_{spec} is a constant of the equipment, the product $C_{\mathrm{spec}}\cdot P(\alpha)$ should be independent of the direction of illumination.

The refractive index is adjusted in order to superimpose the different curves of $C_{\mathrm{spec}}\cdot P(\alpha)$ for the different incidences. The refractive index obtained is not necessarily the optical refractive index of the material. It should be considered as an effective refractive index n_{eff} that allows the modeling of the surface with a microfacet model. Figure 8 illustrates the adjustment of the effective refractive index n_{eff}.

We obtain the effective refractive index n_{eff} of the surface.

Step 2: Fitting the facet normal distribution function P(α) and the constant C_{spec}.

$P(\alpha)$ is a distribution function. Its integral on the half-space must be equal to 1. Now that we know the effective refractive index of the surface, we can express $C_{\mathrm{spec}}\cdot P(\alpha)$ for each of the 4 repetitions on different areas of the sample and the 10 angles of illumination. We have 40 measurements of the function $C_{\mathrm{spec}}\cdot P(\alpha)$. We average the 40 measurements and we separate C_{spec} and $P(\alpha)$ by normalizing $P(\alpha)$ to 1.

Step 3: Validation of the model by reconstruction of the luminance in the plane of incidence.

We validate the values of $C_{\mathrm{spec}}\cdot P(\alpha)$ and n_{eff} by a confrontation of the luminance calculated with the model and the measurement for different directions of illumination (Figure 9).

The model yields satisfactory predictions for matte and glossy black samples.

Figure 9 shows an example of results obtained by inverting the Cook–Torrance model. The microfacet distribution derived from the model adequately predicts the original BRDF measurements.

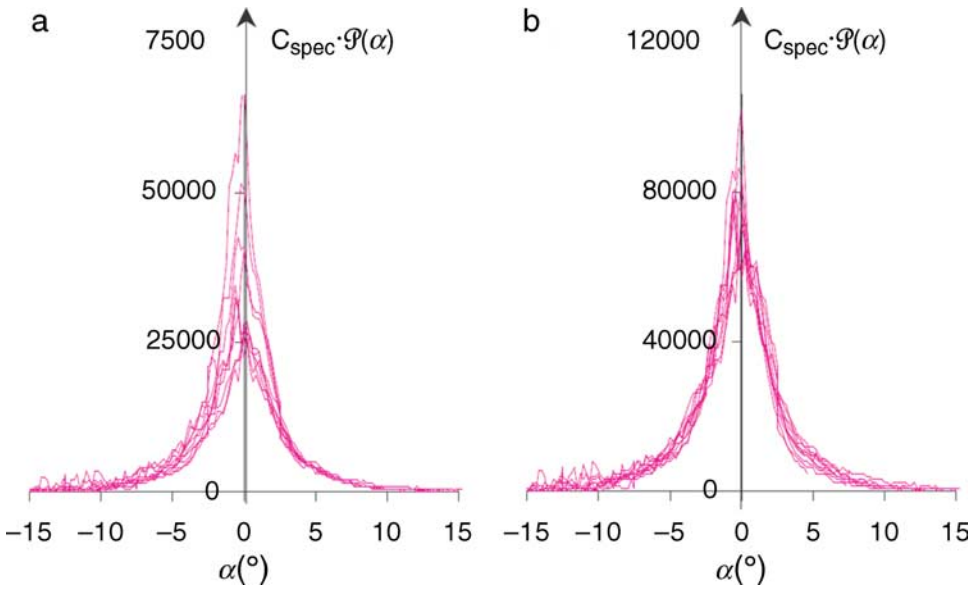

Figure 8. Adjustment method of the refractive index. (a) Peaks before adjustment. (b) Peaks after adjustments.

According to this method, the microfacet distribution $P(\alpha)$ is a function of real BRDF measurements. It is determined by fitting unknowns from the Cook–Torrance model to measurements. Increasing the number of measurements by changing illumination direction is a way to increase the model ability to predict BRDF in every possible direction. Averaging measurements from different parts of the samples adds reliability to the luminance reconstruction obtained in the last stage of the inversion.

This method was applied to each sample, the normalized microfacet distributions of which are drawn in Figure 10.

Analysis of the microfacet distributions

We observe two kinds of behavior for all samples. First, the central part of the distribution is common to all sample measurements. We emphasize that the resolution of the

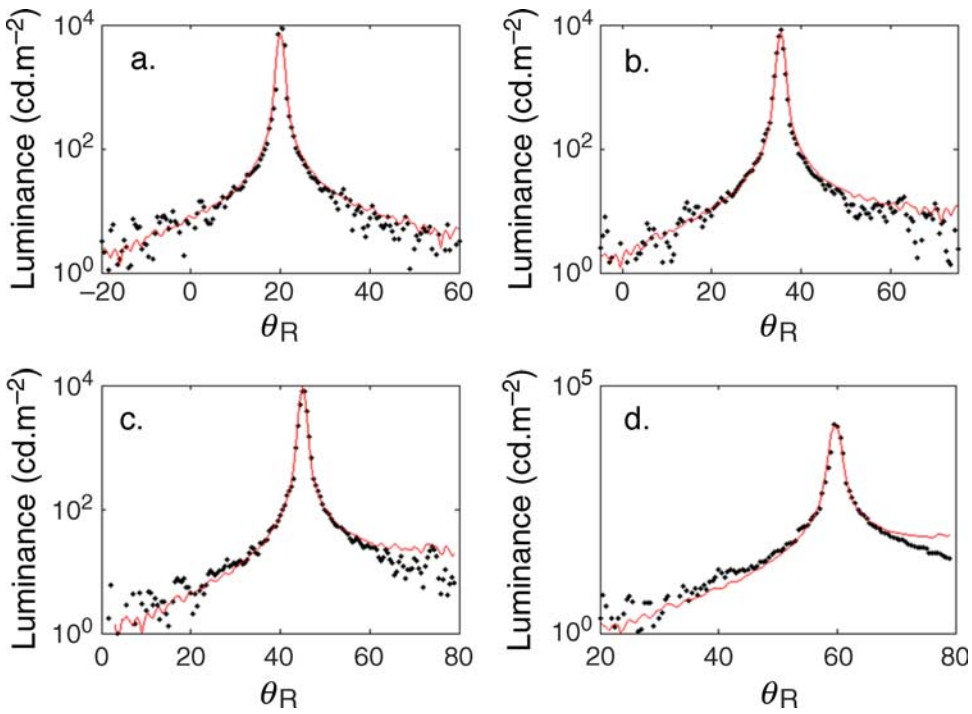

Figure 9. Comparison between model-predicted BRDF (continuous red curve) and measured BRDF (black spots) for sample P1 at incidence of (a) 20°, (b) 35°, (c) 45°, and (d) 60°.

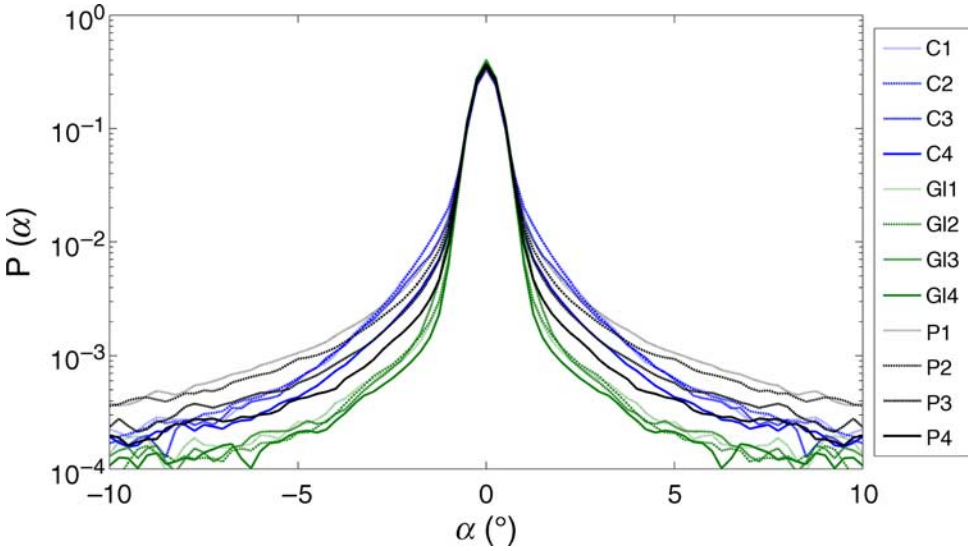

Figure 10. Normalized microfacet distribution. Blue plots stand for C-PMMA, black for P-PMMA, and green for glass samples.

measuring device is not sufficient to detect luminance variations at small angles. Therefore, the bandwidth of this part of the distribution corresponds to the lower limit of the measurable domain of the microfacets attitudes, that is to say ±1.25°. The curves reach the same values and are superimposed on this domain.

The second part of the distribution stretches between 1.25° and wider angles in absolute value. It is specific to each sample. Noise appears in the data for different angles for each sample. For instance, in the case of Glass samples, noise appears for absolute alpha value larger than 5°, whereas PMMA microfacet distributions are smooth up to 8° before showing noisy oscillations at larger angles.

These data are consistent with the results produced by the optical roughness meter. Again, we note a difference between chemical and physical processes. The microfacet distribution, in the case of C-PMMA, is less sharp than for the P-PMMA. Moreover, the two families of curves present two crossovers and are specific to the erosion processes.

The width of each curve is associated to gloss: the narrower the curve, the glossier the sample. Glass samples are the glossiest among the three scales, which is confirmed by gloss index measurements shown in Figure 3. From Figure 10, in order to interpret differences in gloss for the two PMMA sets, it can be expected that gradients, in terms of microfacet distribution slopes, have an impact over the gloss judgment.

Light booth

A preexisting modular light booth was adapted for this experiment (Obein et al., 2004). It allows precise positioning of both samples and light.

Elements of the light booth were designed according to the ASTM standard (ASTM D4449-90, 1990), which recommends a method for visual evaluation of gloss differences between surfaces of similar appearance. The booth is composed of a structure that allows control of the surroundings, a dedicated light, and a stand to manage the geometrical conditions of illumination and viewing.

Six samples are housed in six compartments on a plank that slides on a prop. The prop has a track that allows sample planks to be slotted into it. Samples can then move within the horizontal plane of the booth, left and right from the observer's point of view, conserving their orientation with respect to the illumination. A black velvet paper with two 50 × 40 mm windows separated by a 1-cm margin covered the prop allowing the observer to see two samples at a time. The light booth is shown in Figure 11.

The samples were illuminated by two vertical D65 fluorescent tubes hidden behind a 0.25 × 0.25 inch grid.

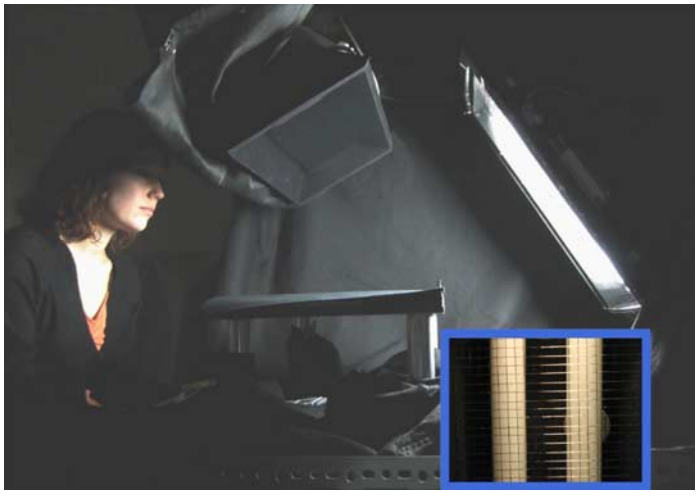

Figure 11. Gloss measurement dedicated light booth. Observers had to slide sample planks under the black velvet paper. The tubes, behind a grid, are shown in the embedded rectangle. Photo: B. Laborie.

The angle between the center of the lamp and the sample prop is 60°. Each viewed sample receives light from the whole length of one vertical tube so that the incidence of the radiations ranges between 80° and 40°. We stress the fact that this configuration produces a different illumination from the one that is defined in the ASTM standard where the fluorescent tubes are horizontal.

Experimental protocol

Our aim was to test whether observers could have access to material substance (i.e., glass vs. PMMA) or structure (i.e., type of depolishing process) through gloss appreciation.

Pair comparison

With 12 samples at our disposal, we used a pair comparison method.

Observers were asked to evaluate a pair of samples illuminated by the two vertical fluorescent tubes. They were free to move their head, so that they could visually explore the region surrounding the specular direction. Observers were asked to select the sample with higher perceived gloss.

Observers

Thirty-three observers aged between 20 and 35 took part in this experiment. All had at least 10/10 corrected near visual acuity and normal stereoscopic vision.

Visual experiment

The test was carried out in four stages.

Vision screening

The observer was screened for near vision acuity using a Parinaud test, stereoscopic acuity using the stereo fly test, and convergence/divergence balance using a Maddox rod.

Collection of vocabulary with two samples

The observer was simultaneously shown the first and last samples from the sanded PMMA scale. He was told that one sample is more "something" than the other and asked to express the difference between the two samples. After he had expressed his own percept of "something," he was told that one of the samples was glossier than the other, and then asked to state which one and to explain his choice.

Pair comparison

The order of presentation of the samples was defined by a Digram-balanced Latin square (Keppel & Wickens, 2004). Each observer began the test with a different order of presentation to balance fatigue effect across samples.

The question (in French) asked to the observer was: "According to you, which is the glossier of these two samples?" The choice was made by the observer in terms of left and right, by pressing two buttons, respectively, located under his left and right hands. While the observer successively answered the five comparisons on each plank, the tester rearranged the samples for the next plank to be presented until the 132 pairs described by the Latin square had been tested. Each pair was presented twice symmetrically with respect to the order of the samples.

The interface of this experiment was developed using LabVIEW and a Lego Mindstorms NXT 2.0 brick to retrieve the observer's choices. The Digram-balanced Latin square was adapted to this language from a preexisting Matlab code developed at the laboratory.

Collection of vocabulary from the subject with six samples

Once the 132 comparisons were performed, the observer was shown simultaneously the first and the last samples from each scale. The objective of this stage was to retrieve his impressions after the test and to establish a table with his own words associated with a given sample.

Principal component analysis

A program converted the choices made by the observer into ones for samples perceived as glossier and zeros for samples perceived as less glossy. A score per sample per observer was obtained from the 132 judgments. Thus, one observer produces a vector of 12 scores. The matrix, consisting of the scores attributed by all observers, is processed with a principal component algorithm (PCA) implemented in Microsoft Excel extension StatBoxPro version 5.0.

Results

Average response

The scores that the observers attributed to samples have led to a ranking, which is compared with the 60° gloss index in Figure 12. The coefficient of determination R^2 is equal to 0.93 indicating a good correlation between appearance and optical measurements.

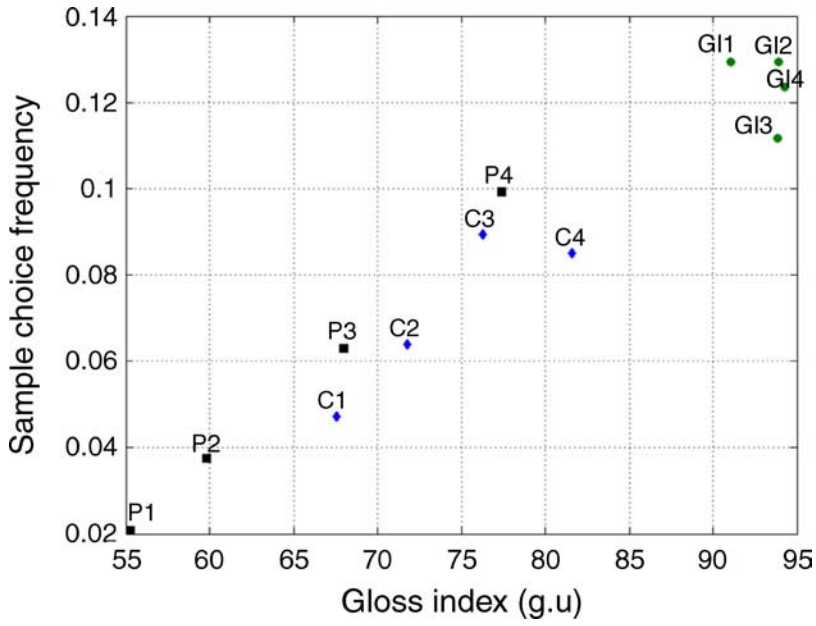

Figure 12. Observers' sample average ranking versus gloss index. Blue diamonds stand for C-PMMA series (C1 to C4), black squares for P-PMMA series (P1 to P4), and green circles for sanded glass series (Gl1 to Gl4). The R^2 coefficient, calculated with Microsoft Excel linear regression tool, is 0.93.

Enunciated vocabulary

The samples that we designed were perceived by the observers as very similar. They often expressed the difficulty to choose between neighboring pallets from the same scale. However, regarding their results and the vocabulary they used, for most comparisons they did not get confused.

When asked to state their criteria for gloss evaluation, they spoke of "sharpness of the illumination reflect" opposed to "amount of light reemitted by the sample."

To compare two samples coming from the same scale, they used color and brightness terms describing shades of blacks or grays.

They referred to sanded glass samples as "greasy, glossy," to sanded PMMA as "sanded, grainy, dusty, glossy," and to chemically depolished PMMA as "glossy, deep, smooth, opaque" (in French). Samples Gl1, P1, and C2 were described as multilayered structures, a glossy material covered with grease for glass samples or a smooth glass superimposed upon surfaces of various roughness for PMMA samples.

Visual data

Eigenvalues of the covariance matrix are represented on the scree plot in Figure 13. We chose to use Kaiser's

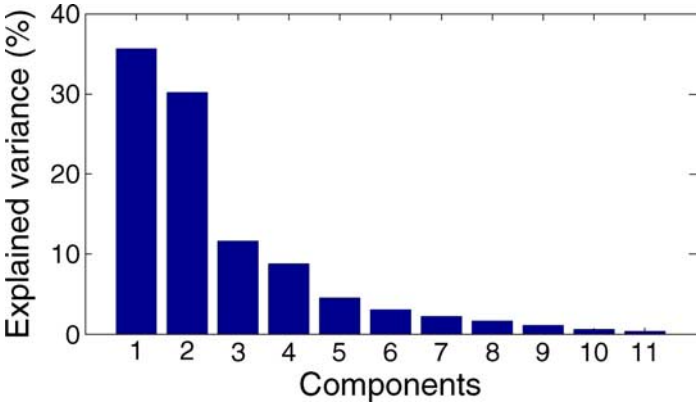

Figure 13. Scree plot of the correlation matrix eigenvalues in terms of explained variance.

Samples	F1	F2	F3	F4
Gl1	0.700	−0.149	−0.372	0.308
Gl2	0.623	0.244	−0.313	0.555
Gl3	0.793	−0.410	0.223	−0.295
Gl4	0.887	−0.220	0.268	−0.221
P1	−0.476	−0.792	0.176	0.111
P2	−0.680	−0.458	0.314	0.347
P3	−0.610	0.400	0.500	0.317
P4	−0.105	0.869	0.270	−0.066
C1	−0.478	−0.749	−0.395	−0.014
C2	−0.666	−0.340	−0.416	−0.324
C3	−0.334	0.705	−0.496	0.081
C4	−0.362	0.635	−0.109	−0.410

Table 1. Sample coordinates within the first four components.

Samples	F1	F2	F3	F4
Gl1	11.457	0.612	9.883	9.004
Gl2	9.067	1.637	7.026	29.140
Gl3	14.701	4.627	3.571	8.264
Gl4	18.379	1.329	5.139	4.643
P1	5.287	17.283	2.207	1.159
P2	10.795	5.784	7.047	11.384
P3	8.703	4.418	17.895	9.486
P4	0.256	20.814	5.224	0.408
C1	5.337	15.482	11.188	0.019
C2	10.361	3.185	12.396	9.958
C3	2.602	13.709	17.573	0.625
C4	3.055	11.120	0.849	15.909

Table 2. Relative contribution of each sample to the first four components.

criterion stating that all eigenvalues above 1 have to be kept. Basing our interpretation on this rule, we explain 86% of the variance using four components.

Sample coordinates are then expressed for each retained component in Table 1.

Knowing the contribution of each of the 12 variables to each component, we can deduce their effect on it. The relative contributions are presented in Table 2.

Tables 1 and 2 show that the first component F1 opposes samples Gl1, Gl2, Gl3, and Gl4 to samples P2, P3, and C2, i.e., the glass samples against specimens from both PMMA physical and chemical sets.

The second component F2 opposes samples P1 and C1 to samples P4, C3, and C4. According to the vocabulary enunciated by the observers, this dimension is associated with color or brightness by the observers.

The third component F3, which only explains a limited amount of variance, opposes samples Gl1, C1, C2, and C3 to sample P3.

These results are shown in Figures 14 and 15. We could not explain the nature of the fourth component and assimilated it to statistical noise. By doing so, we reduced the explained variance to 77%.

Discussion

Correlations between optical and visual measurements

We have tried to relate the data sets issued from optical and visual measurements. On the one hand, optical measurements have yielded multidimensional quantities that the visual system cannot fully access. On the other hand, the subjects of the visual experiment were asked to rank samples according to a single criterion "gloss." It is only after analysis of the physical data that we could expect a reduction of the physical space. In parallel, the PCA of the visual data has revealed several undefined appearance components. Could both analyses of physical and visual data converge? In addition, whereas PCA usually yields dimensions that were not originally included in the description of appearance, could the dimensions extracted from the visual experiment results be related to simple descriptors of the physical observations? Finally, among all available signals, which are the most relevant to surface recognition?

As subjects were free to move their head, they could explore the surroundings of the specular peak as if they were looking for an optimal angular domain to establish their judgment. By doing this, they received the luminance reflected by microfacets at angles different from 0° with respect to the surface normal. We note in Figure 10 that the microfacet distribution intersects several times, so we try to correlate visual ranking with distribution ranking at different angles α.

Calculated correlation coefficients between the optical ranking at every angle and the visual ranking are displayed in Figure 16. The upper left graph shows the correlation coefficients obtained by comparing the sequence of the samples according to the microfacet distributions with the average visual ranking of the samples. In the three other graphs, the correlation coefficients were obtained by comparing the sequence of the samples according to the microfacet distributions with the PCA coordinates of the samples.

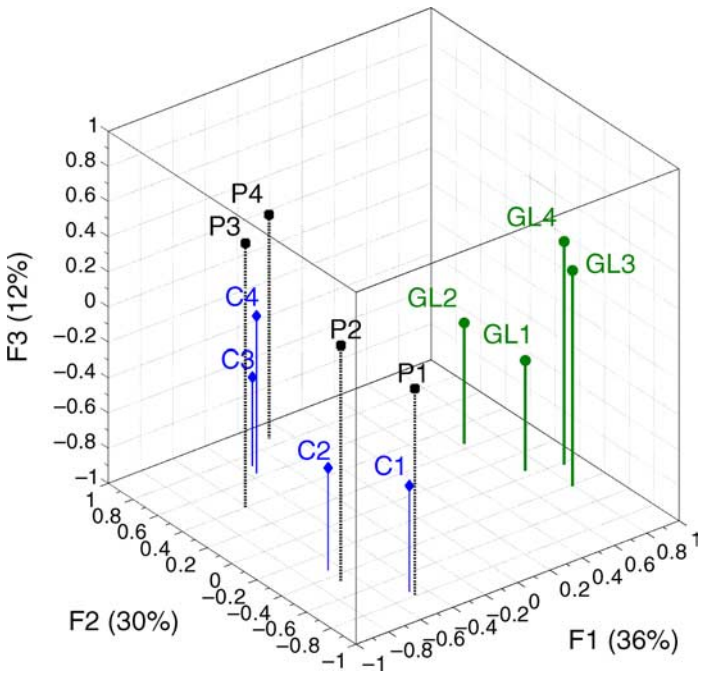

Figure 14. Three-dimensional plot of the PCA results. Thirty-three observers. Blue diamonds stand for PMMA chemical scale, black squares for PMMA physical scale, and green circles for glass scale. Glass samples are distinct from chemically and physically eroded PMMA.

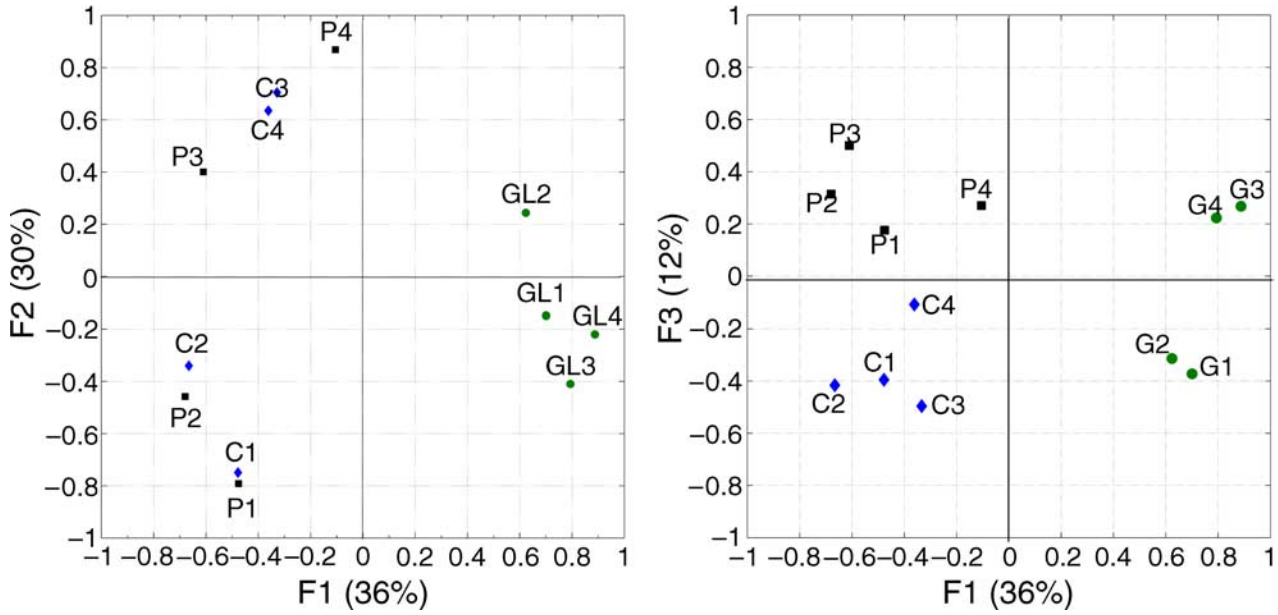

Figure 15. Sample positions regarding components 1 (F1) and 2 (F2) and components 1 (F1) and 3 (F3). Blue diamond stands for PMMA chemical scale, black squares for PMMA physical scale, and green circles for glass scale. Glass samples are distinct from chemically and physically eroded PMMA.

Note that the center correlation coefficients between −1.25° and 1.25° are representative of the instrument function and cannot be safely interpreted. In order to interpret the graphs, it is important to consider the variations in coefficients rather than their instantaneous value.

All graphs show noisy variations out of a ±8° range. The upper left graph "Ranks," comparing the microfacet distribution with the average visual ranking of the samples, allows us to determine the angular limit for noise. We consider that the signal is noisy when the curve starts to

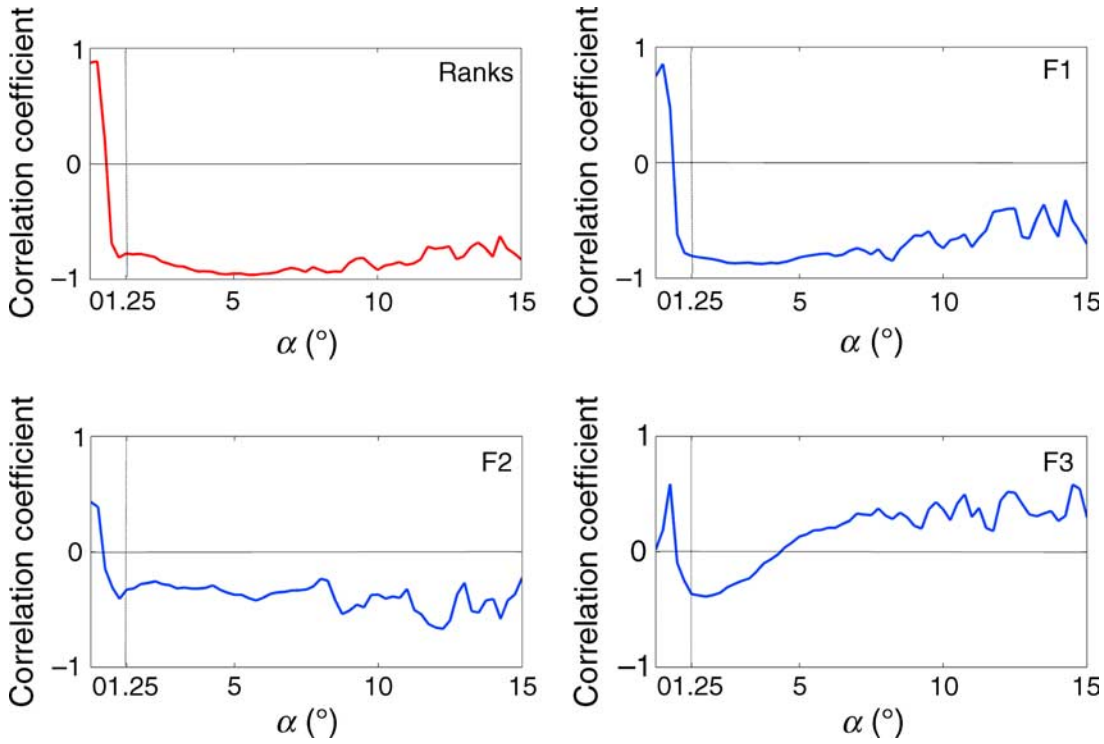

Figure 16. Correlation coefficient between rankings issued from visual experiment and modeled microfacet distributions at several angles.

oscillate. According to this criterion, the significant domain stretches from 1.25° to 8°.

The graph describing F1 reaches a minimum value of −0.8 for the angular domain of 1.25° to 5°. The physical sequence is well correlated with this component over the studied interval. In the graph describing the correlation between F2 and the physical sequence of the samples, the signal is noisier than in the two previous graphs. This could be an effect of the glass samples that are not very reactive to this axis. The fourth graph describes the relation between the component F3 and the physical sequence of the samples for various angles. We observe a sign inversion of the correlation coefficient between 1° and 8°. Light reflection at small or large angles, respectively, associated to DOI or haze, has an opposing effect over component F3. Such sign inversion could represent the duality of the judgment criterion. In fact, when they commented on their strategies, observers reported that they had evaluated samples by either using the distinctness of image of the reflected grid or using a global appreciation of the surface of the bulk material.

Dimensionality

Although it was possible to build a unique scale from the scores given by the observers that vary according to the gloss index (Figure 12), multidimensional analysis clearly reveals the multidimensionality of the glossiness.

At first glance, one might think that first component "F1" discriminates plastic and glass samples over their refractive index, which is a characteristic of the material. However, the difference in terms of refractive index between PMMA and NG9 is too small (0.02) to make such an assumption. It is likely that these two sets of samples are distinguished upon gloss index, glass samples being much glossier than the others as shown in Figures 6 and 12.

The second component "F2" (Figure 15) displays samples in the correct order with respect to the haze of the samples (Figure 3). Glass is scarcely affected by this component.

Lastly, although the variance associated with the third component is low, it is remarkable that the two sets of PMMA are distinguished over "F3," which is probably associated with roughness profiles as these data correlate well with results shown in Figure 4.

This interpretation of the results that were produced by the principal component analysis concurs with microscopy photographs of the plastic samples. Analysis of images from Figure 4 shows an evolution of the surface—for instance, the gloss index decreases when the duration of the erosion process is expanded. This is observed within the same scale of PMMA and for the two different plastic scales. Furthermore, the two plastic scales have typical surface profiles (like the two graphs presented in Appendix A). So they present different roughness and possibly different visual aspects.

In our experiment, although observers could not name the material of the pallets, PCA results indicate that they could use several cues to establish their judgment. The way these cues interact to establish the gloss judgment of the observer is probably complex. Examination of the variances shows that the first two components and the sum of "F3" and "F4" contribute with close weights to the total variance. Such a balance is fragile and may be sensitive to the decision of a few observers.

So, is the observer scrutinizing the surface or is he analyzing the reflected image of the grids and fluorescent tubes? During the experiment, observers were asked to state their criterion for gloss evaluation. We distinguished two categories of judgments. Some observers were evaluating gloss according to the amount of light the surface reflected while others used a distinctness of image criterion, based on the sharpness of the details of the light source image superimposed on the surface. Such a dichotomy was described by Harrison and Poulter (1951). A line is imaged as a line through a polished glass, but the surface when it is abraded has a point spread function of some extent. An observer scrutinizing the surface is collecting the distribution of reflected light wherever it originates from.

We should mention that although visual data produces three components to describe our samples, it does not mean that a single observer would simultaneously use these three cues. PCA was based on covariance across subjects; subsequently, one observer could use only one subset of the proposed dimensions to judge the glossy artifacts he is presented with. It describes dimensions through observers' reactions not through samples themselves.

Subsurface

When Matusik et al. (2003) asked observers to characterize each of the BRDFs from their database using 16 different traits; these included a few terms similar to those spontaneously reported by our observers such as "greasiness" or "dustiness." These terms describe layers superimposed over a surface.

Such subsurface observation can be explained in Figure 10 presenting the result of the inverted microfacet distribution model. We suppose that the apparent duality of the observed surface could be explained as the visual system separating two curves: a function corresponding to a highly specular behavior of a polished surface combined with another function related to roughness. When presented with an unknown material, the observer extracts from the complex BRDF a few components that he can easily relate to previously known object properties.

However, the EZ-Contrast sensor resolution, inferior to 0.4° or 0.002 steradians, which is well under other measurement devices (Matusik et al., 2003), is not sufficient to detect such phenomena. We suppose that data referring to

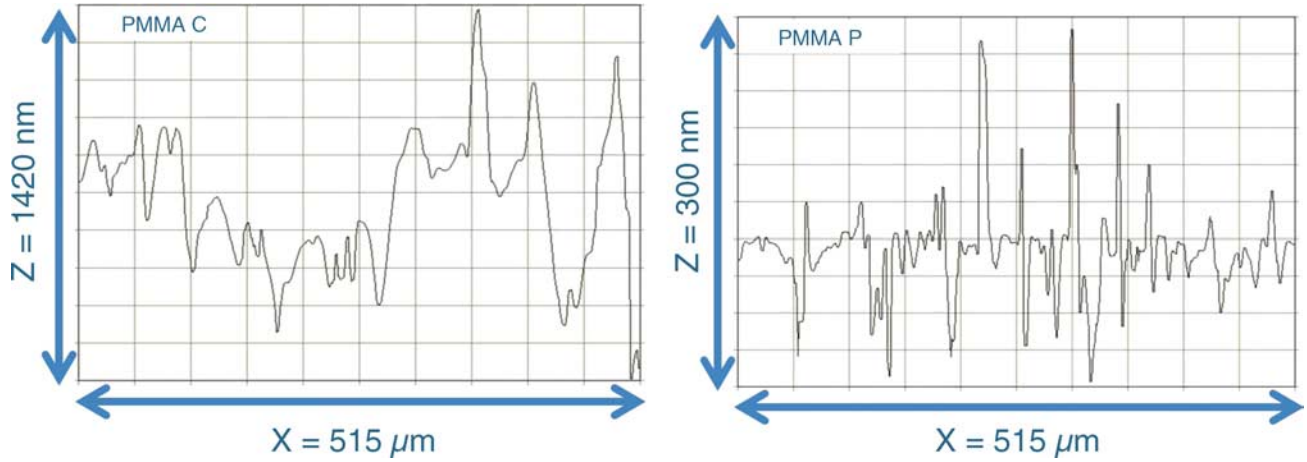

Figure A1. Qualitative characterization of the two PMMA erosion processes. Surface profile on an inline distance of 500 μm. The ordinate axis reaches the value of 790 nm for the left sample (chemically depolished) and 190 nm for the right sample (physically eroded). The horizontal axis is the same in the two graphs (courtesy of Essilor R&D Physique Chimie).

both roughness origins are embedded within the small angular domain that we cannot access, masked by the instrument function. The narrowing of existing goniore-flectometers' resolution will lead to better understanding of such light and surface interactions (Nowbuth, 2008).

Conclusions

Our perception of real objects is issued from an interpretation of a complex combination of physical descriptors. The ability of the visual system to correctly identify objects and materials in the real world is necessary for our survival. As the visual system cannot perform a time-consuming accurate analysis of every perceived physical parameter, it extracts key features of the material, in a global approach. This concern is also of practical importance in industry, as differences in appearance and gloss of materials that are manufactured using the same process are sources of client dissatisfaction that translates in commercial loss. The decision relative to the appearance should therefore be reliable.

Realism is the inescapable constraint. This paper approaches the question through the study of gloss appearance. The assessment of gloss needs an understanding of how an observer assembles the various patterns of light in front of him to obtain a realistic representation of the scene compliant with natural constraints, expected functionality, material and object constancy, and the stability perceived by the viewer of his immediate world. The manner in which the brain has learned to associate optical signals relevant to gloss perception and to material recognition is still a challenge in psychophysical science.

The aim of this study was to investigate the ability of an observer to recognize the microroughness of a surface through visual inspection. We carried out a visual experiment over a limited number of real samples, of different materials and different roughness.

Gloss dimensionality is a recurrent question in both natural and artificial contexts. Our results establish that the visual system is able to select different components within gloss perception. Moreover, it seems that observers could tell that the samples were roughened in different ways. We propose, based on the samples we developed in this paper, three principal components to apprehend gloss. These correlate, respectively, to luminous flux, haze, and microfacet distribution of the surface.

Appendix A

Qualitative description of the surface profile

During the early stages of development of the eroding process, we obtained the spatial profile of the surface from two PMMA items produced by both depolishing processes. These two items were not included in the main study. The graphs presented in Figure A1 illustrate the difference of surface erosion. These graphs were obtained from an Eotech Optosurf interferometric microscope coupled with its treatment software. The left graph represents a chemically attacked pallet whereas the right graph represents a physically eroded PMMA.

Although the amplitudes of the variation of surface level are quite different, they are typical of the processes used to depolish them. The chemical erosion produces smooth curves on the profile graph. The alumina

projections dig up shards of material, thus producing succession of noticeable peaks and valleys (Martin, 2010).

Acknowledgments

This research was supported by the Laboratoire Commun de Métrologie LNE-Cnam and the Centre de Recherche sur la Conservation des Collections. We extend our thanks to Carole Nadolny, Joseph Martin, and Catherine Fauquier from Essilor R&D Physique et Chimie for access to laboratory facilities, to Bertrand Lavédrine from CRCC for advising about the chemical process, to Baptiste Laborie for the Digram algorithm, to Gaëlle Mann from LCM-LNE for technical support, to Kristyn Falkenstern and Lawrence Mac Carthy for linguistic support, to Fatima Benhalima, Thierry Justin, Adrien Bak, and Sophie Vo from CRCC for their previous work, to Ludivine Dechêne from Eldim SA for software support, to the 33 observers who took part in this experiment, to the referees who reviewed this paper and to colleagues from both LCM-Cnam and CRCC.

Commercial relationships: none.
Corresponding author: Guillaume Ged.
Email: guillaume.ged@cnam.fr.
Address: LCM LNE-Cnam, 61 rue du Landy, 93210 La Plaine Saint-Denis, France.

References

ASTM D4449-90 (1990). *Standard test method for visual evaluation of gloss differences between surfaces of similar appearance. ASTM standards on color and appearance measurement* (6th ed.). West Conshohocken, PA: ASTM.

ASTM E430-97 (1997). *Standard test method for measurements of gloss of high gloss surfaces by goniophotometry. ASTM standards on color and appearance measurement* (6th ed.). West Conshohocken, PA: ASTM.

Billmeyer, F. W., & O'Donnell, F. X. D. (1987). Visual gloss scaling and multidimensional scaling analysis of painted specimens. *Color Research and Application, 12,* 315–326.

Blinn, F. (1977). Models of light reflection for computer synthesized pictures. *Proceedings of SIGGRAPH 77, 11,* 192–198.

Bloj, M. G., Kersten, D., & Hurlbert, A. C. (1999). Perception of three-dimensional shape influences colour perception through mutual illumination. *Nature, 402,* 877–879.

Commission Internationale de l'Eclairage (CIE) (2006). *A framework for the measurement of visual appearance*. CIE 175:2006.

Cook, R., & Torrance, K. (1982). A reflectance model for computer. *ACM Transactions on Graphics, 1,* 7–24.

Coutin, J.-M. (2010). LCM-Cnam, France. Personal communication.

Delaney, J. K., de la Rie, E. R., Elias M., Sung L. P., & Morales K. M. (2008). The role of varnishes in modifying light reflection from rough surfaces. *Studies in Conservation, 53,* 170–186.

Elson, J. M., & Bennett, J. M. (1979). Relation between the angular dependence of scattering and the statistical properties of optical surfaces. *Journal of the Optical Society of America, 69,* 31–47.

Fleming, R. W., Dror, R. O., & Adelson, E. H. (2003). Real-world illumination and the perception of surface reflectance properties. *Journal of Vision, 3*(5):3, 347–368, http://www.journalofvision.org/content/3/5/3, doi:10.1167/3.5.3. [PubMed] [Article]

Garcia-Suarez, L., Ruppertsberg, A. I., & Bloj, M. (2008). Visual sensitivity to achromatic gradients with different luminance profiles [Abstract]. *Journal of Vision, 8*(6):942, 942a, http://www.journalofvision.org/content/8/6/942, doi:10.1167/8.6.942.

Gouraud, H. (1971). Computer display of curved surfaces. Department of Computer Science, University of Utah, UTEC-CSc-71-113, June 1971. Also in IEEE Trans. C-20 (June 1971), 623–629.

Harrison, V. G. W., & Poulter, S. R. C. (1951). Gloss measurement of papers—The effect of luminance factor. *British Journal of Applied Physics, 2,* 92–97.

Hunter, R. S., & Harold, R. W. (1987). *The measurement of appearance* (2nd ed.). New York: John Wiley & Sons.

ISO 2813 (1978). *Paint and varnishes: Measurement of the specular gloss of non-metallic paint films at 20°, 60° and 85°*. Geneva, Switzerland: International Organization for Standardization.

Ji, W., Pointer, M. R., Luo, R. M., & Dakin, J. (2006). Gloss as an aspect of the measurement of appearance. *Journal of the Optical Society of America A, 23,* 22–33.

Keppel, G., & Wickens, T. (2004). *Design and analysis. A researcher's handbook* (4th ed.). Upper Saddle River, NJ: Pearson Education.

Koenderink, J., & Pont, S. (2003). The secret of velvety skin. *Machine Vision and Applications, 14,* 260–268.

Kröger, E., & Kretschmann, E. (1970). Scattering of light by slightly rough surfaces or thin films including plasma resonance emission. *Zeitschrift für Physik A Hadrons and Nuclei, 237,* 1–15.

Landy, M. S. (2007). A gloss on surface properties. *Nature, 447,* 158–159.

Martin, J. (2010). Essilor R&D Physique et Chimie. Personal communication.

Matusik, W., Pfister, H., Brand, M., & McMillan, L. (2003). A data-driven reflectance model. *ACM Transactions on Graphics (Proceedings of SIGGRAPH 2003, San Diego, CA, July 27–31), 22,* 759–769.

Moreau, O., Curt, J. N., & Leroux, T. (2000). Contrast and colorimetry measurements versus viewing angle for microdisplays. *Proceedings of SPIE, 4207,* 20–30.

Motoyoshi, I., Nishida, S., & Adelson, E. H. (2005). Image statistics as a determinant of reflectance perception [Abstract]. *Journal of Vision, 5*(8):569, 569a, http://www.journalofvision.org/content/5/8/569, doi:10.1167/5.8.569.

Motoyoshi, I., Nishida, S., Sharan, L., & Adelson, E. H. (2007). Image statistics and the perception of surface qualities. *Nature, 447,* 206–209.

Ng, Y., Zeise, E., Mashtare, D., Kessler, J., Wang, J., Kuo, C., et al. (2003). Standardization of perceptual based gloss and gloss uniformity for printing systems. *Proceedings of the Fifth International Symposium on Multispectral Color Science, 1,* 88–93.

Nowbuth, K. (2008). *Design of a gonioreflectometer* (EiCnam Engineering School Final Report, pp. 11–24). France: Conservatoire National des Arts et Métiers.

Obein, G., Knoblauch, K., & Viénot, F. (2004). Difference scaling of gloss: Nonlinearity, binocularity, and constancy. *Journal of Vision, 4*(9):4, 711–720, http://www.journalofvision.org/content/4/9/4, doi:10.1167/4.9.4. [PubMed] [Article]

Obein, G., Leroux, T., Knoblauch, K., & Viénot, F. (2001). Bidirectionnal reflection factor and gloss scales. *Proceedings of SPIE, 4299,* 279–290.

Obein, G., Leroux, T., Knoblauch, K., & Viénot, F. (2003). Visually relevant gloss parameters. *Proceedings of the 11th International Metrology Congress (Toulon, 20–23 October 2003), 1,* 6.

Obein, G., & Viénot, F. (2007). Modelling the BRDF of a series of matt to glossy black samples. *Proceedings of the CIE Expert Symposium on Visual Appearance, CIE publication x032:2007, 1,* 67–74.

Pellacini, F., Ferwerda, J., & Greenberg, D. (2001). *Toward a psychophysically based light reflection model for image synthesis*. SIGGRAPH 2000, Results appeared in Computer Graphics World, October 2001.

Phong, B. T. (1975). Illumination for computer generated pictures. *Communications of the ACM, 18,* 311–317.

Ruppertsberg, A. I., Bloj, M., & Hurlbert, A. (2008). Sensitivity to luminance and chromaticity gradients in a complex scene. *Journal of Vision, 8*(9):3, 1–16, http://www.journalofvision.org/content/8/9/3, doi:10.1167/8.9.3. [PubMed] [Article]

Smith, K. B. (1997). A sharper look at gloss. *Surface Coatings International Part B: Coatings Transactions, 80,* 573–576.

Te Pas, S. F., & Pont, S. C. (2005). A comparison of material and illumination discrimination performance for real rough, real smooth and computer generated smooth spheres. *Proceedings of the 2nd Symposium on Applied Perception in Graphics and Visualization (August 26–28, 2005, A Coroña, Spain), 1,* 75–81.

Todd, J. T., Norman J. F., & Mingolla (2004). Lightness constancy in the presence of specular highlights. *Psychological Science, 15,* 33–39.

Torrance, K., & Sparrow, E. (1967). Theory for off-specular reflection from roughened surfaces. *Journal of the Optical Society of America, 57,* 1105–1115.

Vangorp, P., Laurijssen, J., & Dutré, P. (2007). The influence of shape on the perception of material reflectance. *ACM Transactions on Graphics (Proceedings of SIGGRAPH 2007), 26,* 77.

Viénot, F., Boust, C., Brémond, R., & Dumont, E. (2002). Rating tone-mapping algorithms for gradations. In *The First European Conference on Color in Graphics Imaging and Vision (CGIV), April 2002, Poitiers, France* (vol. 1, pp. 221–225). Springfield, USA: IS&T.

Viénot, F., & Obein, G. (2004). Is Gloss recognized as a surface property? *Proceedings of MS 2004, 1st International Workshop on Materials and Sensations (Pau, France, 27–29 October 2004), 1,* 77–82.

Ward, G. J. (1992). Measuring and modelling anisotropic reflection. *Computer Graphics, 26,* 265–272.

Wills, J., Agarwal, S., Kriegman, D., & Belongie, S. (2009). Toward a perceptual space for gloss. *ACM Transactions on Graphics, 28,* 103:1–103:15.

Xiao, B., & Brainard, D. H. (2008). Surface gloss and color perception of 3D objects. *Visual Neuroscience, 25,* 371–385.

Zerrouki, C. (1998). *La rugosité nanométrique des surfaces polies: Etude expérimentale par diffusion de la lumière. Application à l'étude des étalons de masse en alacrite XSH*. PhD, Conservatoire National des Arts et Métiers, France.